Journal of Catalysis **182,** 165–173 (1999)
Article ID jcat.1998.2322, available online at http://www.idealibrary.com on IDEAL®

Reduction of Nitric Oxide by Isobutene over Cu–Mn Alloys

H. Lu,* C. M. Pradier,†,[1] and U. O. Karlsson*

*Materials Physics, Royal Institute of Technology, 100 44 Stockholm, Sweden; and †Laboratoire de Physico-chimie des Surfaces, CNRS-UPRESA 7045, Ecole Nationale Supérieure de Chimie de Paris, 11 rue Pierre et Marie Curie, 75005 Paris, France

Received July 1, 1998; revised November 4, 1998; accepted November 4, 1998

Cu–Mn alloys with various bulk compositions have been used in the catalytic reduction of NO by i-C_4H_8 at 500°C. The gas-phase reactions were monitored by mass spectroscopy (MS) and the catalyst surfaces were characterized by X-ray photoelectron spectroscopy (XPS) at certain stages of the reactions. The compositions and oxidation states of the alloy surfaces are strongly dependent on the bulk composition and the oxygen pressure, and eventually influence the reaction kinetics, product distribution, as well as mechanism of NO reduction. On a Cu–Mn (atomic 8%) alloy surface, with a medium oxygen pressure (reducing conditions), the reaction of NO with partially oxidized products of i-C_4H_8 is suggested to be the main mechanism of NO reduction. However, too low or too high an oxygen pressure leads to direct decomposition of NO with the production of N_2 or N_2O, depending on reducing or oxidizing reaction conditions. On high-manganese-concentration alloy surfaces (55%, 92% atomic), under strong reducing conditions, the main path of NO reduction is via the reaction of adsorbed NO_2 with i-C_4H_8, which gives rise to N_2 production. When the reaction conditions pass from reducing to oxidizing, NO decomposition leads to the formation of N_2O. © 1999 Academic Press

Key Words: **NO reduction; hydrocarbon; Cu–Mn alloy; surface segregation; X-ray photoelectron spectroscopy.**

1. INTRODUCTION

Interest in heterogeneous catalysis by alloys is stimulated by the fact that alloying modifies the ensemble and electronic state of the alloy constituents, thus causing substantial changes in the surface properties and reactivities (1). Therefore, alloys are expected to exhibit synergistic effects, possibly leading to new catalysts or precursors of new catalysts with high activity and selectivity.

Compared with pure metals, using alloys as catalysts brings out some additional problems (2). First, the surface segregation leads to different surface composition as compared with the bulk alloy. Second, the properties of alloy surfaces cannot be regarded as a simple combination of the corresponding characteristics of the pure constituents. Moreover, one component of the alloy may undergo a selective oxidation, which makes the surface composition sensitive to the atmosphere (e.g., more or less oxidizing). So, it is generally accepted that a catalytic study of alloys should be accompanied by a careful analysis of the alloy surface composition and its oxidation level, which are the conditions necessary to characterize the active sites and explain the reaction mechanism (3).

In a previous paper, we studied the reduction of NO by isobutene over a copper surface (4). It was revealed that NO conversion proceeds via two stages: a stage of slow NO conversion, in which an active intermediate (i-C_4H_6O) is produced on the Cu(I) oxide, and then a stage of rapid reduction of NO by i-C_4H_6O on the metallic Cu surface. As a continuation of our previous work, we report in this paper a study of the reduction of NO by isobutene on Cu–Mn alloy surfaces. The Cu–Mn system was chosen in this study for a number of reasons. First, both elements have been intensively used in NO_x catalysis (4, 5 and references therein); mixed copper–manganese oxides and Hopcalite catalyst, $CuMn_2O_4$, show high reactivity in the removal of NO and N_2O (6–9). Second, it is known that both Cu and Mn can form more than one oxide, and their oxides are mutually soluble to some extent; therefore, the Cu–Mn alloy surface promises interesting catalytic properties (2). Third, for Cu–Mn alloy, it has been established that there is a large hybridization between Cu 3*d* and Mn 3*d* electrons in Cu–Mn bonding (10), and the authors predicted that such unusual hybridization may lead to substantial effects in the alloy surface properties. The oxygen and sulfur dioxide adsorption study on a Cu(100)–c(2×2)–Mn surface alloy, which shows greatly enhanced reactivity of the Cu–Mn surface alloy relative to a pure Cu surface, supports this proposal (11).

This work aims at providing preliminary information about Cu–Mn alloy catalysts in NO_x applications. Special attention is addressed to monitor the change in alloy surface compositions and oxidation levels as a function of the bulk compositions and also the reaction conditions. The variations in the surface characteristics will be correlated to the activity, the selectivity, and the mechanism of NO

[1] To whom correspondence should be addressed. Fax: 33-1-4634 0753. E-mail: pradier@ext.jussieu.fr.

0021-9517/99 $30.00

reduction. Such a model approach is facilitated by the use of planar catalysts, three bulk alloys having different initial concentrations.

2. METHODS

The catalysts used in this study were Cu–Mn alloy sheets, each with a surface area of 32 cm^2. The bulk compositions of the alloys were 8, 55, and 92% Mn, respectively (in the text, all percentages are atomic percentages). The alloys were provided by Goodfellow Cambridge Limited. Before each test, the catalyst sample was reduced in hydrogen with a pressure of 10 Torr (1 Torr = 133.3 N m^{-2}) at 500°C for 1 h.

The gas mixtures used in the reactions were NO (1.0 Torr), i-C_4H_8 (0.5 Torr), and O_2 (0–3.1 Torr). $P_{O_2} <$ 2.5 Torr corresponds to reducing conditions regarding the total oxidation of hydrocarbon, and $P_{O_2} > 2.5$ Torr, to oxidising conditions. Ar was added as a balance gas to maintain a total pressure of 5.0 Torr. All catalytic reactions were performed at 500°C. The activity of a reaction is evaluated by the time required to convert 30% of the initial NO amount, i.e., $T_{30\%}$.

A detailed description and schematic outline of the experimental system were reported in a previous paper (12). Catalytic experiments were performed in a batch mode reactor. A mass spectrometer was used to monitor the gas-phase compositions during the reaction process; the quantitative mass spectrometry (MS) data were evaluated using the fragmentation patterns determined experimentally from calibration gases (12).

For the concerned reactions, the catalyst surfaces were characterized by X-ray photoelectron spectroscopy (XPS). To do so, the reaction was interrupted when 30% NO was converted; the reactor was quenched to room temperature and then evacuated, and the catalyst was transferred through an ultrahigh vacuum line to a surface analysis chamber. In the XPS measurement, Mg$K\alpha$ (1253.6 eV) radiation was used as the X-ray excitation source, and the electron kinetic energies were analyzed by a CLAM 2 hemispherical energy analyzer with a pass energy of 20 eV. The binding and kinetic energies in the text were referred to the $4f_{7/2}$ core level of gold, a small sample of which was coated on the sample holder. The value of Au $4f_{7/2}$ was taken as 84.0 eV. The intensities of all the spectra were measured after background subtraction.

3. RESULTS

3.1. NO Conversion on Cu–Mn Alloy Surfaces

Reactions of NO and i-C_4H_8 in the presence of oxygen were successively tested over the Cu–Mn (8%), Cu–Mn (55%), and Cu–Mn (92%) alloys. Identical initial conditions were used: $P_{NO} = 1.0$ Torr, $P_{i\text{-}C_4H_8} = 0.5$ Torr, $P_{O_2} = 1.0$ Torr, Ar as a balance gas, $T = 500$°C. Figure 1 shows the changes in gas compositions during the catalytic reactions on the three alloy surfaces.

In the initial 15–30 min of each catalytic test (region A in Fig. 1), the temperature of the reactor was raised from room temperature to 500°C, the gas mixture was homogenized, and the reaction between O_2 and i-C_4H_8 was initiated. After this primary period, the conversion of NO took place. The main products of the reaction were N_2, CO_2, and H_2O. Time for 30% NO conversion, $T_{30\%}$, was 70, 110, and 175 min for Cu–Mn (8%), Cu–Mn (55%), and Cu–Mn (92%), respectively.

To compare the alloy activities with that of a pure copper catalyst, a copper sheet with the same surface area was also tested for NO reduction under the same initial conditions; the $T_{30\%}$ was 88 min.

In addition to the changes in NO conversion rate ($T_{30\%}$), different features appeared in the reactions catalyzed by low-Mn-content alloy (8%) and high-Mn-content alloys (55 and 92%). On the Cu–Mn (8%) surface, NO conversion proceeded via two stages: a slow followed by a rapid conversion stage (marked as stages I and II in Fig. 1a). CO and i-C_4H_6O were produced in stage I, and the amounts of both i-C_4H_6O and CO quickly decreased in stage II. It should also be noted that the CO_2 and H_2O concentrations monotonously increased throughout the reaction (even after total disappearance of oxygen in the gas phase). The reaction catalyzed by the pure copper catalyst surface showed similar trends (figure not shown).

Conversely, NO was converted in one stage on either Cu–Mn (55%) or Cu–Mn (92%) catalyst. CO and i-C_4H_6O were hardly detectable during the whole reaction process. On the Cu–Mn (92%) alloy, the rate of the formation of CO_2 and H_2O was strongly correlated to the presence of O_2 in the gas phase: very strong at the beginning of the reaction and drastically reduced after complete consumption of gas phase oxygen. The conversion of NO was significant only after complete consumption of oxygen. On the Cu–Mn (55%) alloy, CO_2 and H_2O behavior was intermediate, and NO conversion was initiated when half the amount of oxygen was consumed.

3.2. Influence of O_2 Pressure

The influence of oxygen pressure on NO reduction has been investigated on three alloy surfaces. P_{O_2} was varied from 0 to 3.1 Torr, i.e., from reducing to oxidizing conditions as defined under Experimental. Other conditions were kept the same as in Fig. 1.

Figure 2 shows the dependence of $T_{30\%}$, which varies in the sense opposite to the activity, on the initial pressure of oxygen for the three alloys. On the Cu–Mn (8%) alloy surface, the rate of NO conversion decreased when the oxygen pressure increased. On the Cu–Mn (55%) and Cu–Mn (92%) alloy surfaces, addition of a small amount of

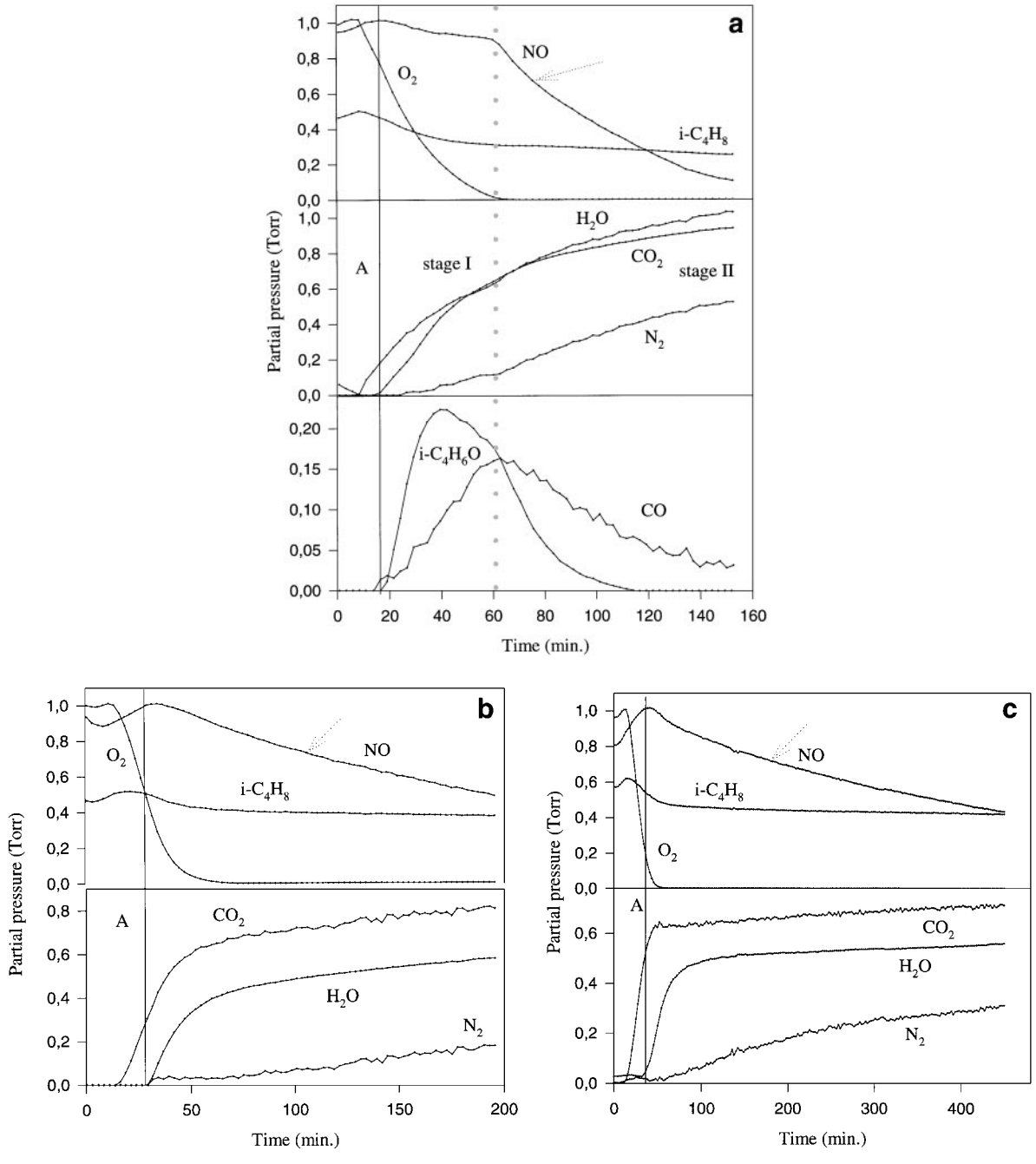

FIG. 1. Time courses of NO, O_2, i-C_4H_8, N_2, CO_2, H_2O [CO and i-C_4H_6O in (a)] in the reactions catalyzed by (a) Cu–Mn (8%), (b) Cu–Mn (55%), and (c) Cu–Mn (92%). $P_{NO} = P_{O_2} = 1.0$ Torr, $P_{\text{i-}C_4H_8} = 0.5$ Torr, $P_{Ar} = 2.5$ Torr, $T = 500°$C. "A" indicates the initial period of the reaction. The arrow shows the time when XPS measurement was performed.

O_2 to the reaction gas mixtures significantly enhanced the rate of NO conversion, but "too high" oxygen pressures ($\geq$0.6 Torr) led to weaker activity.

Furthermore, on the Cu–Mn (8%) surface, the time course of the reactions varied with the initial oxygen pressure (figures not shown). As we reported in the preceding section, when the oxygen pressure was 1.0 Torr, two NO conversion stages were observed, associated with the formation and consumption of CO and i-C_4H_6O intermediate products. However, with too low (0 to 0.6 Torr,) or too high (3.1 Torr) oxygen pressures, NO concentration monotonously decreased; CO and i-C_4H_6O could not be detected. On the two other alloy surfaces, a "one-stage" NO conversion was observed whatever the oxygen

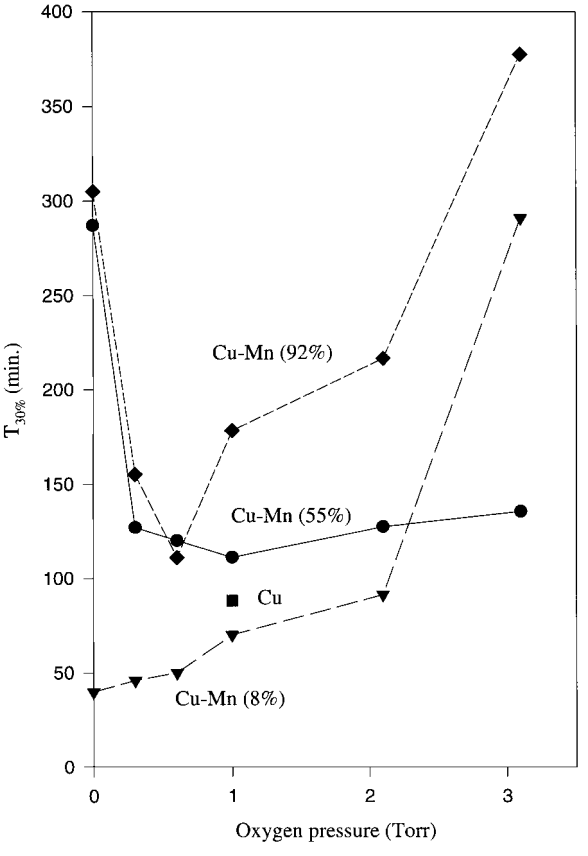

FIG. 2. $T_{30\%}$ as a function of oxygen pressure over different alloy surfaces. $P_{NO} = 1.0$ Torr, $P_{i\text{-}C_4H_8} = 0.5$ Torr, Argon as balance gas maintaining a total pressure of 5.0 Torr, $T = 500°C$.

pressure, without any correlation with CO or i-C_4H_6O formation.

Note also that, on all alloy surfaces, under reducing conditions ($P_{O_2} < 2.5$ Torr), NO was converted mainly to N_2. Under oxidizing conditions ($P_{O_2} = 3.1$ Torr O_2), immediate formation of water and carbon dioxide was observed, followed by the production of N_2O.

3.3. Surface Characterization

XPS measurements have been performed on three alloy surfaces, at initial O_2 pressures of 0, 1.0, and 3.1 Torr, the reaction being interrupted at 30% NO conversion; the other reaction conditions were the same as in Fig. 1.

Figure 3 shows the Cu 2*p*, Cu LMM, Mn 2*p*, O 1*s*, and C 1*s* X-ray photoelectron spectra taken from the Cu–Mn (8%) surface. It has been well established that Cu(0) and Cu(I) show similar Cu 2*p* binding energies, but have different kinetic energies for Cu LMM Auger lines (13). We can thus conclude from Figs. 3a and 3b that Cu is mainly in the metallic state whatever the oxygen pressure. When P_{O_2} is equal to 3.1 Torr, a shoulder at 916.4 eV in the Cu LMM spectrum C indicates the presence of a small fraction of Cu(I) on the surface.

Figure 3c shows the corresponding Mn 2*p* core levels. Whatever the reaction conditions, the high binding energy of the Mn $2p_{3/2}$ peak indicates that no metallic Mn is present (14). In spectra A and B (corresponding to reducing reaction conditions), the satellites around 647.5 eV are characteristic of Mn^{2+} (15), showing the existence of MnO on the surface. In spectrum C ($P_{O_2} = 3.1$ Torr, oxidizing conditions), the satellite around 647.5 eV disappears. The onset of the Mn $2p_{3/2}$ line remains in the same position and the $2p_{3/2}$ peak broadens to high binding energy with a decrease in its total intensity, indicating a decrease in Mn^{2+} surface concentration to the benefit of manganese in a higher oxidation state. However, the broad Mn $2p_{3/2}$ peak makes it difficult to distinguish between different oxides. Note that for Mn^{x+} ($x > 2$), the oxidation level cannot be identified by Mn 2*p* satellites, since the Mn $2p_{3/2}$ satellites overlap with the Mn $2p_{1/2}$ peak, and, when Mg$K\alpha$ is used, the Mn $2p_{1/2}$ satellites overlap with the Mn LMM Auger line (15).

With a change in oxygen pressure, no essential variation in the O 1*s* spectra is observed (Fig. 3d). Two contributions can always be used to fit the peak: a main one at 529.9 eV and a small one at 531.7 eV. The 529.9-eV peak can be assigned to oxygen in oxides, which grows when the oxygen pressure increases. The one at higher binding energy is attributed to adsorbed hydroxyl groups (16, 17).

In Fig. 3e, the C 1*s* spectrum A shows a broad emission centered at 284.8 eV, which can be attributed to different carbonaceous species. With an increase in the oxygen pressure, the C 1*s* peak decreases (spectrum B) and finally disappears under oxidizing conditions (spectrum C).

The X-ray photoelectron spectra taken of the Cu–Mn (55%) and Cu–Mn (92%) surfaces are not shown. The same features and evolution are observed for the O 1*s* and C 1*s* peaks as a function of oxygen pressure. Table 1 shows the oxidation levels of copper and manganese, deduced from the binding energies of the Cu 2*p* and Mn 2*p* core levels and kinetic energy of the Cu LMM Auger lines, for the three alloy surfaces under different initial oxygen pressure conditions. The changes in oxidation states of the alloys, whether there is 8, 55, or 92% manganese, lie mainly in the copper under oxidizing conditions: Cu is partially oxidized to Cu^+ in the 8% Mn alloy and to Cu^{2+} in the other alloys. Note that under reducing conditions the Cu LMM Auger lines of Mn 55% and 92% alloys are too weak to differentiate Cu^+ from Cu^0.

FIG. 3. X-ray photoelectron spectra taken from Cu–Mn (8%) surface: (a) Cu 2*p*; (b) Cu LMM Auger line; (c) Mn 2p (arrows show the Mn $2p_{3/2}$ satellites); (d) O 1*s*; (e) C 1*s*. $P_{O_2} = 0$, 1.0, and 3.1 Torr in spectra A, B and C respectively. Argon as balance gas maintains a total pressure of 5.0 Torr. Other reaction conditions are the same as in Fig. 1.

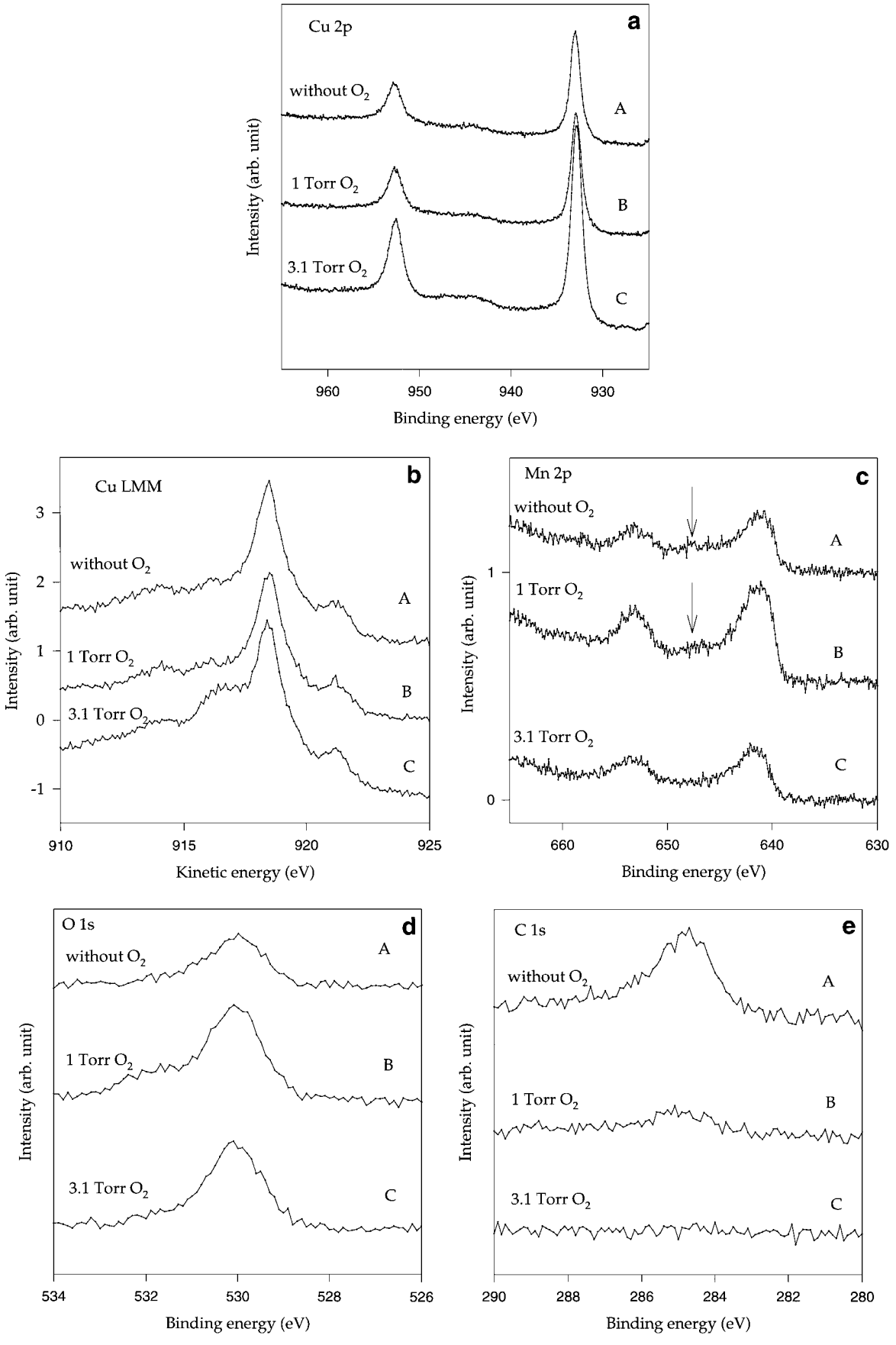
Cu 2p
a
without O_2
A
1 Torr O_2
B
3.1 Torr O_2
C
Intensity (arb. unit)
960
950
940
930
Binding energy (eV)
Cu LMM
b
without O_2
A
1 Torr O_2
B
3.1 Torr O_2
C
Intensity (arb. unit)
3
2
1
0
-1
910
915
920
925
Kinetic energy (eV)
Mn 2p
c
without O_2
A
1 Torr O_2
B
3.1 Torr O_2
C
Intensity (arb. unit)
1
0
660
650
640
630
Binding energy (eV)
O 1s
d
without O_2
A
1 Torr O_2
B
3.1 Torr O_2
C
Intensity (arb. unit)
534
532
530
528
526
Binding energy (eV)
C 1s
e
without O_2
A
1 Torr O_2
B
3.1 Torr O_2
C
Intensity (arb. unit)
290
288
286
284
282
280
Binding energy (eV)

TABLE 1

Oxidation States of Alloy Surfaces under Different Oxygen Pressure Conditions

	Bulk Mn concentration		
P_{O_2}	8%	55%	92%
0 Torr	Cu^0 Mn^{2+}	Cu^0 and/or Cu^+ [a] Mn^{2+}	Cu^0 and/or Cu^+ [a] Mn^{2+}
1 Torr	Cu^0 Mn^{2+}	Cu^0 and/or Cu^+ [a] Mn^{2+}	Cu^0 and/or Cu^+ [a] Mn^{2+}
3.1 Torr	Cu^0, Cu^+ Mn^{x+} ($X \geq 2$)	Cu^{2+} Mn^{x+} ($X \geq 2$)	Cu^{2+} Mn^{x+} ($X \geq 2$)

[a] The Cu LMM Auger line is too weak to give essential information; thus Cu^0 and Cu^+ cannot be differentiated.

3.4. Determination of Alloy Surface Compositions

The compositions of the top layers of the alloys under different initial oxygen pressure conditions have been estimated by XPS data. The intensities of the Cu $2p_{3/2}$ and Mn $2p_{3/2}$ lines are taken as the areas of the peaks excluding satellite lines. The calculation of the values of the superficial concentrations is based on a model that considers a homogeneous enrichment (or depletion) throughout several superficial layers of the oxide (18). This approximation has been made for sake of simplification though we are aware of the possible alternation of rich and poor Mn layers in the case of an important segregation (19). In fact, our objective is to characterize the tendency of Mn segregation to alloy surfaces when submitted to various oxygen pressures and, above all, to compare the results for the three alloys having different bulk concentrations of manganese. This was of course to help in the interpretation of the observed differences in their catalytic behavior.

The superficial concentration of Mn and Cu could be deduced according to the classical formula

$$\frac{I_{Cu}}{I_{Mn}} = \frac{\lambda_{Cu}}{\lambda_{Mn}} \frac{Y_{Cu}}{Y_{Mn}} \frac{D_{all}^{Cu}}{D_{all}^{Mn}} \frac{e^{-d/\lambda_{Cu}} + D_0^{Cu}(1 - e^{-d/\lambda_{Cu}})}{e^{-d/\lambda_{Mn}} + D_0^{Mn}(1 - e^{-d/\lambda_{Mn}})},$$

d being the thickness of the modified alloy (Å). λ_i is the mean free path of the $2p_{3/2}$ of the i element electron in the alloy; it can be obtained by assuming that the lattice is only slightly modified by alloying and using the formula $\lambda_i = 0.41a\sqrt{a}E_c$, where a is the lattice parameter and E_c is the kinetic energy of the emitted electrons from the considered level. The following values are obtained: $\lambda_{Cu} = 7.6$ Å, $\lambda_{Mn} = 10.5$ Å (for the $2p_{3/2}$ core levels). Y_i, the photoelectric yield of element i, is proportional to the cross section, characteristic of the element and of the considered level; values are given by well-established tables. D_{all}^i is the concentration of i in the modified alloy, and D_0^i is the concentration of i in the bulk alloy.

Table 2 gives the values of concentrations and corresponding thicknesses of an alloy modified by segregation through its first 5 or 10 first layers, determined from a computerized calculation. When two sets of values are given, it means that a more or less large number of modified layers can be considered to account for the XPS data.

The results show the following:

(1) Segregation of Mn is observed on all samples; it is maximum under low oxygen pressure (1 Torr).

(2) Whatever the pressure of oxygen, the Cu–Mn (55%) alloy exhibits an almost pure Mn surface. This is also true for the 92% Mn alloy in the presence of low oxygen pressure.

(3) For the 8 and the 92% alloys, when $P_{O_2} = 3.1$ Torr, the segregation of Mn is reduced.

Note that our calculation does not consider the oxidation of copper and manganese. In fact, the surface alloy top layers consist of a mixture of copper (copper oxide) and manganese oxides, depending on the conditions as shown in Table 1, covering a bulk alloy. A calculation, made by assuming a number of oxide layers having an average density close to that of Cu_2O, was tested; it did not lead to significant differences in the surface segregation quantification. Moreover, the Mn percentage values, issued from our calculation, are probably overestimated due to the fact that we did not include a contribution from the layers, which have been Mn-depleted by the segregation phenomenon. Actually, the heterogeneity in the top several layers in different alloys has been evidenced in the literature (20). Being aware of these restrictions, one will keep in mind that the active surfaces are all enriched in manganese under reaction conditions. An exception was made clear for the 92% Mn alloy, where a copper-over-manganese peak ratio corresponding to the bulk composition is observed when $P_{O_2} = 3.1$ Torr.

TABLE 2

Concentrations and Thicknesses of the Modified Alloys under Different Initial Oxygen Pressure Conditions (Results from a Computerized Model)

	Bulk Mn concentration		
P_{O_2}	8%	55%	92%
0 Torr	32% over 5 layers or 24% over 10 layers	≈Pure Mn over 5 or 10 layers	≈Pure Mn over 5 layers or 97% over 10 layers
1.0 Torr	45% over 5 layers or 38% over 10 layers	≈Pure Mn over 5 or 10 layers	≈Pure Mn over 5 layers or 98% over 10 layers
3.1 Torr	14% over 5 layers or 13% over 10 layers	≈Pure Mn over 5 or 10 layers	89% over 5 or 10 layers

4. DISCUSSION

4.1. Surface Segregation and Oxidation Phenomena

The surface composition changes of different alloys as a function of oxygen pressure observed by XPS can be interpreted by considering the tendency of each element to form oxide (thermodynamic effect) and their diffusion coefficient in the bulk alloy (kinetic effect) (2 and references therein). Mn has a higher affinity to oxygen and Mn oxides are more stable than copper oxides. However, copper diffuses more rapidly than manganese. The segregation phenomenon, which is not strictly governed either by thermodynamics or by cation size effect, strongly depends on the reaction conditions and the bulk composition of the alloy.

Table 1, reporting the oxidation states of the alloys, suggests a first comment: oxidation of the surface, and of Mn in particular, occurs even in the absence of oxygen or under reducing conditions; this confirms the affinity of Mn for oxygen and the stability of Mn oxide.

For a low-Mn-concentration alloy, Cu–Mn (8%), whatever the pressure of oxygen, a preferential oxidation of Mn (Mn^{x+}, $x \geq 2$) is observed, whereas copper remains in the metallic state or is partially oxidized to Cu_2O. This selective oxidation is accompanied by segregation of Mn toward the surface as indicated in Table 2.

Under reducing conditions ($P_{O_2} < 2.5$ Torr), the Mn surface concentration increases to a value as high as 45% in a five-layer model. In the absence of oxygen, Mn is obviously oxidized by NO which decomposes at the surface. The surface behavior can be interpreted by analogy with the oxidation of Cu–Mn (10%) alloy under low oxygen pressure conditions reported by Yoon and Cocke (2): the reaction gas mixture provides a mild oxidizing atmosphere, under which the oxidation and segregation behavior is controlled by thermodynamics. The higher Gibbs free energy of the Mn oxide compared with that of copper oxide leads manganese to be oxidized first [$G_f(Cu_2O) = -146.4$ kJ/mol and ($G_f(MnO) = -363.2$ kJ/mol] (2). In fact, though conditions are "reducing" in the sense of complete combustion of isobutene, Mn oxide is formed by interaction of oxygen and is stable, whereas Cu_2O, if formed, tends to decompose at the reaction temperature (21). As a consequence, oxygen and/or NO in the gas phase promote Mn segregation by a preferential Mn oxidation.

Under oxidizing conditions ($P_{O_2} = 3.1$ Torr), manganese is further oxidized (Mn^{x+}, $x \geq 2$), and its segregation is reduced compared with that under reducing conditions. Some oxidized copper (Cu_2O) has been detected. Yoon and Coke observed a similar phenomenon with a 10% Mn alloy at high O_2 exposure. They explained that the first stage of oxidation of Cu–Mn alloy is expected to be a simultaneous formation of Cu and Mn oxides. Due to the preferential oxidation of Mn, a Mn-depleted region is induced in the top layers, so the subsequent Mn oxidation is controlled by its diffusion rate in the alloy. Now, Cu oxide grows more rapidly because of the higher Cu concentration in the top layers, resulting in reduced Mn segregation to the surface, where two oxide phases eventually coexist.

For a medium Mn concentration, Cu–Mn (55%), whatever the pressure of oxygen, the surface layers are strongly enriched in manganese oxide. Copper is detected by XPS in the metallic and/or Cu_2O forms under reducing conditions and in the CuO form under oxidizing conditions. This again shows that thermodynamics controls the alloy surface behavior, favoring a selective oxidation of manganese. As a matter of fact, Mn is always at an oxidation level higher than that of coexisting copper; and copper oxide does not overgrow Mn oxide due to the high enough bulk concentration of manganese.

For the Mn-rich alloy, the surface is almost pure manganese oxide under reducing conditions. The striking observation is the absence of Mn segregation under oxidizing conditions, leading to a higher copper oxide surface concentration compared with what was observed under reducing conditions. A possible explanation can be suggested. For the high-Mn-concentration alloy, the large hybridization bond between Cu 3*d* and Mn 3*d* strongly modifies the chemical properties of Cu, e.g., its oxygen affinity in this case. Thus, under oxidizing conditions, Cu and Mn are both rapidly oxidized. Equilibrium is rapidly reached between the topmost oxide layers and the bulk alloy without significant Mn segregation.

4.2. Catalytic Activity

XPS data and the above discussion give us an insight into the copper–manganese ratio and the oxidation level of the alloy surfaces at 30% NO conversion of each considered reaction. Although these data vary when the reaction proceeds, kinetics results, in particular the NO conversion curve and reaction products as well as the influence of oxygen pressure, can be tentatively correlated to the surface characterization.

4.2.1. Cu–Mn (8%) Alloy

a. $P_{O_2} = 1$ Torr (reducing conditions). Figure 1a shows that the reaction takes place following the same "two-stage" feature as on a pure copper surface (4). For the same reasons as on the pure copper, the reaction of NO with i-C_4H_6O and CO is suggested to be the main path for NO conversion.

Note that the rate of NO conversion is promoted on the alloy compared with that on the pure copper surface. This could be explained by the mild oxidizing properties of the manganese oxide which favors the formation of active intermediates, i.e., CO and i-C_4H_6O. It has been shown by Yang *et al.* that, for CO oxidation, mixed copper–manganese oxides are considerably less active than copper oxide (22, 23).

b. $P_{O_2} < 1$ Torr (strongly reducing conditions). The XPS data show that, with no oxygen in the gas phase, the surface is less Mn-enriched compared with that in the presence of 1 Torr of oxygen (see Table 2). On the surface, copper is in the metallic state, whereas manganese is oxidized to the 2+ state. Under strong reducing conditions, the kinetic data show that the rate of NO conversion slightly increases when P_{O_2} decreases and NO is continuously converted to the benefit of N_2; i.e., there is no initial stage. This leads us to assume a change in the main path of the reaction compared with the previous case. We tentatively suggest that the direct decomposition of NO into N_2 dominates the reaction. The inhibitory effect of O_2 on the rate of NO conversion, in that range of pressure, can be explained by that oxygen competing with NO for adsorption sites. The role of hydrocarbon is to prevent further oxidation of the surface, i.e., to keep a proper environment for the decomposition of NO. As a comparison, the direct decomposition of NO is known to be catalyzed by MnO, Mn_2O_3, and Mn_3O_4 surfaces at 500°C (24, 25). The dissociative adsorption of NO on metallic copper surfaces is well documented in the literature (26). Considering the respective reactivities of Cu(0) and Mn oxides, the reactivity of the 8% Mn alloy (∼20–30% Mn on the surface) for NO decomposition is not surprising under the present conditions. Note that this is the main path of the reaction only when the initial oxygen pressure is low in the gas phase ($P_{O_2} < 1$ Torr), i.e., when the surface is composed mainly of metallic copper and manganese oxide.

c. $P_{O_2} = 3.1$ Torr (oxidizing conditions). Under the present conditions, the surface Mn concentration is close to that of the bulk, ca. 13%; the surface is strongly oxidized; Cu/Cu^+ and Mn^{x+} ($x \geq 2$) coexist. This oxidized surface is likely to promote deep oxidation of isobutene to the detriment of NO direct decomposition and of the reaction of NO with HC or with an intermediate. Once the combustion of the hydrocarbon is over, NO starts to react significantly and produces N_2O as the main product. NO is likely to react with the manganese oxide surface via the reaction $2NO + MnO_x \rightarrow N_2O + MnO_{x+1}$ (5).

d. Summary. The Cu–Mn (8%) alloy is slightly more reactive than a pure copper surface. Its reactivity changes with oxygen pressure; this is due to a change in surface compositions and oxidation levels as well as to kinetic factors. With low oxygen pressures (0–0.6 Torr, strong reducing conditions), a very reactive Cu–Mn alloy surface leads to direct decomposition of NO. Oxygen competes with NO for adsorption sites and thus inhibits the rate of NO conversion. The role of the hydrocarbon is to prevent deep oxidation of the surface. A medium oxygen pressure generates a surface and a gas-phase environment that favor partial oxidation of hydrocarbon. Thus, reaction of i-C_4H_6O and CO with NO is the main path of the reaction. A high oxygen pressure (oxidizing conditions) induces strong oxidation of the surface components, which favors the combustion of i-C_4H_8. In this case, NO is converted mainly to N_2O.

4.2.2. Cu–Mn (55%) and Cu–Mn (92%) Alloys

a. $P_{O_2} = 0$–1 Torr (reducing conditions). Under reducing conditions, a continuous decrease in NO without a preliminary stage to the exclusive benefit of H_2O, CO_2, and N_2 is always observed. On none of these surfaces, does partial oxidation of isobutene seem to occur. When a small amount of oxygen is present in the reactants, the conversion of NO is significantly more rapid (Fig. 2); note that this is not the case with the Cu–Mn (8%) alloy surface. The rate of NO conversion reaches a maximum at $P_{O_2} = 0.6$ or 1 Torr for the 92 and 55% alloys, respectively. To interpret these kinetic data, one has to consider the surface compositions under the reaction conditions. XPS shows that although the bulk Cu/Mn ratios are very different between these two alloys, the active surfaces of both alloys are almost pure manganese oxide. With the change in oxygen pressure, both surfaces are not significantly changed either in the surface compositions or in the oxidation levels.

Here, it is worth mentioning the work of Aylor *et al.* on NO reduction by methane over Mn-ZSM-5 (5). Observing the surface NO_2 species by infrared, the authors suggested that the reduction of NO proceeds via the formation of NO_2 and the subsequent reduction of adsorbed NO_2 by CH_4. Under our reaction conditions, considering that the alloy surfaces are almost pure manganese oxides, we thus tentatively suggest a similar reaction. Several comments are given here. (1) NO_2, as a surface intermediate, is not detected in the gas phase. (2) The significant increase in NO conversion rate by the presence of a small amount of O_2 can be explained by the promotion of the formation of surface NO_2 species. (3) The decline in the NO conversion rate with further increase in oxygen pressure can be explained by the combustion of i-C_4H_8, a parallel reaction competing with NO for the surface oxygen. Note that the combustion of CH_4 by oxygen is also observed over Mn-ZSM-5 (5). (4) At "high" oxygen pressure, when the formation of NO_2 surface is inhibited, replaced by the combustion of i-C_4H_8, we do not exclude the possibility that a direct NO decomposition could also occur.

b. $P_{O_2} = 3.1$ Torr (oxidizing conditions). Under oxidizing conditions, the rate of NO conversion decreases and N_2O is produced over both surfaces. With the same arguments as developed above for the Cu–Mn (8%) alloy, we assume that highly oxidized surfaces first promote the combustion of isobutene and then lead to the reaction of NO into N_2O.

c. Summary. On the two Mn-rich Cu–Mn alloys, the active surfaces behave as pure manganese. With an increase in oxygen pressure, the rate of NO conversion passes

through a maximum for $P_{O_2} = 0.6$ or 1 Torr, under which the formation of reaction intermediate NO_2 is most promoted. Reaction of NO_2 with i-C_4H_8 is the main path of NO reduction. With a further increase in oxygen pressure (still reducing conditions), the combustion of i-C_4H_8 is accelerated. The rate of NO conversion is consequently decreased. When the reaction conditions pass to oxidizing, complete combustion of hydrocarbon and conversion of NO to N_2O are observed.

5. CONCLUSION

In this paper we studied NO reduction by i-C_4H_8 at 500°C over Cu–Mn (8%), Cu–Mn (55%), and Cu–Mn (92%) surfaces using MS and XPS. It is revealed that, under reducing conditions, the reactivity on different surfaces follows the sequence Cu–Mn (8%) > Cu > Cu–Mn (55%) > Cu–Mn (92%). It is also demonstrated that the surface composition of the alloys can be very different from that of the bulk depending on the reaction conditions.

On the Cu–Mn (8%) surface, enriched in manganese 13 to 45%, depending on the reaction conditions, changes in the mechanism of NO reduction were made clear. Without oxygen or with a low oxygen pressure, direct NO decomposition to N_2 is suggested to be the main mechanism. With a medium oxygen pressure (slightly reducing conditions), the partial oxidation of i-C_4H_8 is, as on a pure copper, the initial step of the reaction; it is followed by a reaction of NO with oxygenated intermediates. Under oxidizing conditions, NO reacts with the surface oxides, leading to N_2O as the main product.

On the Cu–Mn (55%) and Cu–Mn (92%) alloys, the reactive surfaces are almost pure manganese oxide. Under reducing conditions, the NO reduction proceeds via the oxidation of NO to NO_2 and the subsequent reduction of adsorbed NO_2 by i-C_4H_8. Under oxidizing conditions, NO decomposition leads to N_2O production.

Our results shows how complex it is to use alloys as catalysts due to considerable variations in the surface concentrations after segregation. Oxygen pressure and bulk composition influence the oxidation level as well as the surface composition. It is consequently essential to characterize the chemical state of the surface to be able to interpret the kinetic data. In the case of Cu–Mn alloys, Mn tends to migrate to the surface, resulting in a complex effect on the activity, selectivity, and even mechanism of the reaction. For NO reduction by a hydrocarbon, the best system seems to be an alloy having a very low manganese loading (8% in our example) which exhibits a higher activity than a pure copper.

ACKNOWLEDGMENTS

We are grateful to the Swedish National Board for Industrial and Technical Development (NUTEK) and the Swedish Natural Science Research Council (NFR) for their support for this research.

REFERENCES

1. Ponec, V., *Surf. Sci.* **80**, 352 (1979).
2. Yoon, C., and Cocke, D. L., *Appl. Surf. Sci.* **31**, 118 (1988).
3. Sachtler, W. M. H., and Van Santen, R. A., *Adv. Catal.* **26**, 69 (1977).
4. Lu, H., Pradier, C. M., and Flodström, A. S., *J. Mol. Catal.* **112**, 447 (1996).
5. Aylor, W., Lobree, L. J., Reimer, J. A., and Bell, A. T., *J. Catal.* **170**, 390 (1997).
6. Wöllner, A., Lange, F., Schmelz, H., and Knözinger, H., *Appl. Catal. A Gen.* **94**, 183 (1993), and references therein.
7. Panayotov, D., *React. Kinet. Catal. Lett.* **58**, 73 (1996).
8. Dermott, J. M. C., *in* "Pollution Control Review," Vol. 2. Noyes Data Corp., Park Ridge, IL, 1971.
9. Lawrence, A., *in* "Pollution Control Review," Vol. 8. Noyes Data Corp., Park Ridge, IL, 1972.
10. Steiner, P., Hufner, S., Martensson, N., and Johansson, B., *Solid State Commun.* **37**, 73 (1981).
11. Lu, H., Janin, E., Davila, M., Pradier, C. M., and Göthelid, M., *Surf. Sci.* **408**(1–3), 326 (1998).
12. Lu, H., Pradier, C. M., and Karlsson, U. O., *J. Mol. Catal.*, in press.
13. Larsson, P. E., *J. Electron Spectrosc.* **4**, 213 (1974).
14. Moulder, J. F., Stickle, W. F., Sobol, P. E., and Bomben, K. D., "Handbook of X-ray Photolectron Spectroscopy," p. 79. Perkin-Elmer Corp., 1992.
15. Di Castro, V., and Polzonetti, G., *J. Electron Spectrosc.* **48**, 117 (1989), and references therein.
16. Spitzer, J., and Lüth, H., *Surf. Sci.* **160**, 353 (1985).
17. Robert, T., Bartel, M., and Offergeld, G., *Surf. Sci.* **33**, 123 (1972).
18. DeVito, E., and Marcus, P., *Surf. Interf. Anal.* **19**, 403 (1992).
19. Bertolini, J. C., Massardier, J., Delichere, P., Tardy, B., Imelik, B., Jugnet, Y., Duc, T. M., De Temmerman, L., Creemers, C., Van Hove, H., and Neyens, A., *Surf. Sci.* **119**, 95 (1982).
20. Nanni, P., Viani, F., Elliott, P., and Gesmundo, F., *Oxidation Metals* **13**(2), 181 (1979).
21. Hegde, M. S., *Appl. Surf. Sci.* **17**, 97 (1983).
22. Yang, L., Chan, S. F., Chang, W. S., and Chen, Y. Z., *J. Catal.* **130**, 52 (1991).
23. Wood, J., Wise, H., and Yolles, R., *J. Catal.* **15**, 355 (1969).
24. Yamashita, T., and Vannice, A., *J. Catal.* **163**, 158 (1996).
25. Luo, M. F., Zhou, L. H., and Zheng, X. M., *Indian. J. Chem. A Inorg.* **35**(1), 53 (1996).
26. Balkenende, R., Hoogendam, R., de Beer, T., Gijzeman, O. L. J., and Geus, J. W., *Appl. Surf. Sci.* **55**, 1 (1992).